

# PLANETARY CAPTURE USING LOW-THRUST PROPULSION

Dilmurat AZIMOV<sup>1</sup>

Robert H. BISHOP

*The Center for Space Research  
The University of Texas at Austin  
Austin, TX, 78712*

*Email: azimov@csr.utexas.edu*

*Email: rhbishop@mail.utexas.edu*

**ABSTRACT**—*The variational problem of determining low-thrust planar planetary capture trajectories in a central Newtonian field is considered. Analytical solutions previously obtained for variable specific impulse and constant power propulsion systems are presented in a form convenient for application to the planetary capture problem. The solutions describe a family of low-thrust spiraling trajectories terminating on a given elliptical parking orbit. By analyzing the optimality conditions at the junction between the low-thrust capture spiral and the elliptic parking orbit, it is shown that extremal low-thrust trajectories can be described completely analytically if the initial range of the spacecraft, perigee and apogee of the parking orbit, maximum level of power, efficiency of the propulsion system and final mass are specified. A numerical example confirms the results.*

**KEYWORDS**—Variational problem, low-thrust, optimal trajectories, planetary capture, analytical solutions.

## INTRODUCTION

In this paper we consider the variational problem of optimal planetary capture trajectories of a spacecraft with low-thrust propulsion. It is known that a space trajectory with constraints on exhaust velocity and mass-flow rate may contain zero thrust (ZT), intermediate thrust (IT), and maximum thrust (MT) arcs [1]. Previous studies of such motion have often considered chemical propulsion systems, which generally are high-thrust, low specific impulse devices. It is also known that in the case of constraints on power and exhaust velocity one can obtain a trajectory containing either zero power (ZP) or maximum power (MP) arcs with variable or constant thrust [2]. Power and exhaust velocity constraints are generally associated with low-thrust, high specific impulse propulsion (i.e., power-limited solar electric, electromagnetic plasma, or ion propulsion systems). Consideration of power and exhaust velocity constraints together in one problem statement allows for the generalization of the variational problem to include the characteristics of both high-thrust and low-thrust propulsion systems. The analysis of the constraints on direction of thrust, power, and specific impulse in the variational statement leads to classes of trajectories that may contain combinations of ZP, intermediate power (IP), and MP arcs with constant and variable specific impulse depending on values of certain control variables and Lagrange multipliers [3]. It is important to note that the system of equations of such a generalized problem can be written in a canonical form which allows the application of many of the methods of analytical mechanics developed for Hamilton dynamic systems. Therefore, the solutions of the canonical equations obtained for ZT, IT and MT arcs in the case of chemical propulsion

---

<sup>1</sup>Associate Professor, Department of Theoretical and Applied Mechanics, Tashkent State University, Tashkent 700095, Uzbekistan. Currently a Research Fellow at the Center for Space Research

systems can also be considered for the low-thrust propulsion systems. This implies the utilization of known relationship between power, mass-flow rate, and exhaust velocity [3].

Investigations of optimal space trajectories with power and exhaust velocity constraints using methods of numerical optimization and nonlinear programming have been reported in the literature (see for example [4]–[5]). Fuel-optimal trajectories for spacecraft using low-thrust variable specific impulse have been given more attention in connection with studies on power-limited round-trip human mission to Mars [6]–[8]. The focus of this paper, however, is not on the application of numerical methods to the solution of the optimal space trajectory problem, but rather on the search for optimal solutions that can be described entirely analytically. The authors have shown that the extremal trajectory with variable specific impulse and constant power can be described entirely analytically (see [3] and [9]). In the present paper it will be shown that the variable specific impulse and constant power analytic solution can be applied to the problem of planetary capture to an elliptical parking orbit.

## PROBLEM STATEMENT

The motion of a spacecraft is considered to be a point mass moving in the central Newtonian field. The dynamics are described by the vector differential equation [3]:

$$\dot{\mathbf{x}} = \mathbf{f}(\mathbf{x}, \mathbf{u}) \quad (1)$$

where the state vector  $\mathbf{x}$  and dynamics  $\mathbf{f}$  are given by

$$\mathbf{x} = \begin{bmatrix} \mathbf{r} \\ \mathbf{v} \\ m \end{bmatrix} \quad \text{and} \quad \mathbf{f}(\mathbf{x}, \mathbf{u}) = \begin{bmatrix} \mathbf{v} \\ -\frac{\mu}{r^3}\mathbf{r} + \frac{2P}{I_{sp}gm}\mathbf{l} \\ -\frac{2P}{I_{sp}^2g^2} \end{bmatrix},$$

and where  $\mathbf{r}$  is the spacecraft position (km),  $\mathbf{v}$  is the velocity (km/s),  $m$  is the mass of the spacecraft (kg),  $\mathbf{l}(l_1, l_2, l_3)$  is the unit thrust vector,  $g$  is the sea-level gravitational acceleration ( $\text{m/s}^2$ ),  $I_{sp}$  is the specific impulse (s),  $\mu$  is the gravitational parameter of the central body ( $\text{km}^3/\text{s}^2$ ),  $P$  is the exhaust power (kw), and the piecewise continuous control vector is denoted by  $\mathbf{u} = (I^T, P, I_{sp})$ . The goal is to transfer the spacecraft from the initial state at  $t_0$

$$\mathbf{r}(t_0) = \mathbf{r}_0, \quad \mathbf{v}(t_0) = \mathbf{v}_0, \quad m(t_0) = m_0, \quad (2)$$

to the final state at  $t_1$

$$\mathbf{r}(t_1) = \mathbf{r}_1, \quad \mathbf{v}(t_1) = \mathbf{v}_1, \quad (3)$$

while minimizing the performance index

$$\mathcal{J} = \frac{1}{2} \int_{t_0}^{t_1} a^2(t) dt, \quad (4)$$

subject to constraints

$$\begin{aligned} h_1 &:= l_1^2 + l_2^2 + l_3^2 - 1 = 0 \\ h_2 &:= P(P_{max} - P) - \gamma^2 = 0 \\ h_3 &:= (I_{sp_{max}} - I_{sp})(I_{sp} - I_{sp_{min}}) - \eta^2 = 0 \end{aligned} \quad (5)$$

where  $a$  is the thrust acceleration given by

$$a = \frac{2P}{I_{sp}gm}.$$

The variables  $\eta$  and  $\gamma$  are treated as auxiliary components of the control vector, therefore,  $\mathbf{u}$  is augmented to include  $\eta$  and  $\gamma$ , so that now  $\mathbf{u} = [\mathbf{1}^T P I_{sp} \eta \gamma]^T$ . The stationarity conditions (or Euler-Lagrange equations) may be expressed as [1]

$$\begin{aligned} \dot{\boldsymbol{\lambda}} + \left[ \frac{\partial \mathbf{f}}{\partial \mathbf{x}} \right]^T \boldsymbol{\lambda} - \left[ \frac{\partial \mathbf{h}}{\partial \mathbf{x}} \right]^T \boldsymbol{\nu} &= 0 \\ - \left[ \frac{\partial \mathbf{f}}{\partial \mathbf{u}} \right]^T \boldsymbol{\lambda} + \left[ \frac{\partial \mathbf{h}}{\partial \mathbf{u}} \right]^T \boldsymbol{\nu} &= 0 \end{aligned} \quad (6)$$

where  $\boldsymbol{\nu}(\nu_1, \nu_2, \nu_3)$  are the Lagrange multipliers,  $\boldsymbol{\lambda} = [\boldsymbol{\lambda}_r^T, \boldsymbol{\lambda}_v^T, \lambda_7]^T$ ,  $\boldsymbol{\lambda}_r(\lambda_4, \lambda_5, \lambda_6)$  is the Lagrange multiplier conjugated to spacecraft position,  $\boldsymbol{\lambda}_v(\lambda_1, \lambda_2, \lambda_3)$  is the primer vector conjugated to the velocity,  $\lambda_7$  is a multiplier conjugated to the mass, and the components of  $\mathbf{h} = [h_1, h_2, h_3]^T$  are given in Eq. (5).

Analysis of the corresponding stationary conditions yields [3]:

$$\begin{aligned} \dot{\boldsymbol{\lambda}}_r &= \frac{\mu}{r^3} \boldsymbol{\lambda}_v - 3 \frac{\mu}{r^5} (\boldsymbol{\lambda}_v^T \mathbf{r}) \mathbf{r} \\ \dot{\boldsymbol{\lambda}}_v &= -\boldsymbol{\lambda}_r \\ \dot{\lambda}_7 &= \frac{2P}{cm^2} \boldsymbol{\lambda}_v^T \mathbf{1} \end{aligned} \quad (7)$$

where  $c = gI_{sp}$  (km/s) is the exhaust velocity, and

$$\begin{aligned} -\frac{2}{cm} \boldsymbol{\lambda}_v^T \mathbf{1} + \frac{2}{c^2} \lambda_7 + \nu_2 (P_{max} - 2P) &= 0 \\ \frac{2P}{c^2 m} \boldsymbol{\lambda}_v^T \mathbf{1} - \frac{4P}{c^3} \lambda_7 + \frac{\nu_3}{g} (I_{sp_{max}} - 2I_{sp} + I_{sp_{min}}) &= 0 \\ -\frac{2P}{cm} \boldsymbol{\lambda}_v + 2\nu_1 \mathbf{1} &= 0 \\ -2\gamma \nu_2 &= 0 \\ -2\eta \nu_3 &= 0. \end{aligned} \quad (8)$$

Note that the third equation of Eq. (8) implies that the vector  $\boldsymbol{\lambda}_v$  is parallel to the direction of thrust  $\mathbf{1}$ , that is

$$\mathbf{1} = \frac{\boldsymbol{\lambda}_v}{\lambda_v}.$$

From the Weierstrass condition, it follows that

$$\frac{P}{c} \left( \frac{\boldsymbol{\lambda}_v^T \mathbf{1}}{m} - \frac{\lambda_7}{c} \right) \geq \frac{\tilde{P}}{\tilde{c}} \left( \frac{\boldsymbol{\lambda}_v^T \tilde{\mathbf{1}}}{m} - \frac{\lambda_7}{\tilde{c}} \right) \quad (9)$$

where  $\tilde{P}$ ,  $\tilde{c}$ , and  $\tilde{\mathbf{1}}$  are admissible values. Suppose that  $\tilde{c} = c$  and  $\tilde{\mathbf{1}} = \mathbf{1}$ , that is, let  $\tilde{c}$  and  $\tilde{\mathbf{1}}$  assume their optimal values. Then, the switching function, denoted by  $\chi$ , and given by

$$\chi = \frac{\lambda_v}{m} - \frac{\lambda_7}{c}$$

is a continuous function, and from Eq. (9) it follows that

$$\frac{\chi}{c} (P - \tilde{P}) \geq 0. \quad (10)$$

Then, taking into account the continuity of  $\boldsymbol{\lambda}^T \dot{\mathbf{x}}$ , it follows that  $P = P_{max}$  when  $\chi > 0$ ,  $P = 0$  when  $\chi < 0$ , and  $0 < P < P_{max}$  when  $\chi = 0$ . Using Eq. (8), it follows that several classes of extremals may exist, such as:

- Null thrust arcs with  $P = 0$  when  $\gamma = 0$ ,  $\nu_2 \neq 0$  and  $\chi < 0$
- Maximum power arcs with  $P = P_{max}$  when  $\gamma = 0$ ,  $\nu_2 \neq 0$  and  $\chi > 0$
- Variable power arcs with  $0 < P < P_{max}$  when  $\gamma \neq 0$ ,  $\nu_2 = 0$  and  $\chi = 0$

and

- Constant  $I_{sp}$  with  $I_{sp} = I_{spmax}$  or  $I_{sp} = I_{spmin}$  when  $\eta = 0$  and  $\nu_3 \neq 0$
- Variable  $I_{sp}$  that satisfies  $I_{spmin} < I_{sp} < I_{spmax}$  when  $\eta \neq 0$  and  $\nu_3 = 0$

All possible combinations of values of  $P$  and  $I_{sp}$  have been mentioned in works [3], [9].

Note that the case of variable  $P$  and variable  $I_{sp}$  is not possible under the problem statement considered here. Indeed, in this case, we have  $\gamma \neq 0, \nu_2 = 0, \eta \neq 0$  and  $\nu_3 = 0$ . From the first and second equations in Eq. (8), it follows that

$$\frac{\lambda_v}{m} - \frac{\lambda_7}{c} = 0$$

and

$$\frac{\lambda_v}{m} - 2\frac{\lambda_7}{c} = 0.$$

This leads to  $\lambda_7 = 0$  which implies that  $\lambda_v = 0$ . This is a contradiction to the statement of the variational problem and to the theory of primer vectors. Consequently, the combination of variable  $P$  and variable  $I_{sp}$  is not further considered as the case of an extremal motion.

In this paper, the class of trajectories corresponding to the case where  $\gamma = 0$ ,  $\eta \neq 0$ ,  $\nu_2 \neq 0$  and  $\nu_3 = 0$  that describes extremal motion with maximum level of power and variable specific impulse will be presented. This corresponds to  $\lambda_v = \sqrt{\lambda_1^2 + \lambda_2^2} = \text{constant}$ . The main equations of the problem being considered and integral expressions are given in the next section. For more details and derivations the reader is referred to the previous work of authors [3].

## EQUATIONS OF THE PROBLEM AND INTEGRAL EXPRESSIONS

The equations of motion Eq. (1) and the stationarity conditions Eq. (8) may be rewritten in the canonical form [3]:

$$\dot{\mathbf{x}} = \left[ \frac{\partial H}{\partial \boldsymbol{\lambda}} \right]^T \quad \text{and} \quad \dot{\boldsymbol{\lambda}} = - \left[ \frac{\partial H}{\partial \mathbf{x}} \right]^T \quad (11)$$

with the Hamiltonian

$$H = \mathbf{f}^T \boldsymbol{\lambda} = -\frac{\mu}{r^3} \boldsymbol{\lambda}_v^T \mathbf{r} + \boldsymbol{\lambda}_r^T \mathbf{v} + \frac{P_{max}}{2b} \lambda_v^2$$

where vectors are given in the planar coordinate system with the origin at the center of attraction [9]:

$$\mathbf{r}(r, 0), \quad \mathbf{v}(v_1, v_2), \quad \boldsymbol{\lambda}_v(\lambda_1, \lambda_2), \quad \boldsymbol{\lambda}_r(\lambda_4; \lambda_1 \frac{v_2}{r} - \lambda_2 \frac{v_1}{r} + \frac{\lambda_5}{r})$$

It can be shown that the system Eqs. (11) has the following first integrals

$$\begin{aligned}
-\frac{\mu}{r^3}\boldsymbol{\lambda}_v^T \mathbf{r} + \boldsymbol{\lambda}_r^T \mathbf{v} + \frac{P_{max}}{2b}\lambda_v^2 &= C \\
I_{sp}gm\lambda_v &= 2b \\
\boldsymbol{\lambda}_v^T \mathbf{v} - 2\mathbf{r}^T \boldsymbol{\lambda}_r - \left(\frac{5P_{max}}{2b}\lambda_v^2 - 3C\right)t &= C_1 \\
\lambda_5 &= C_2,
\end{aligned} \tag{12}$$

and the invariant relations

$$\begin{aligned}
\lambda_1\lambda_4 + \lambda_1\lambda_2\frac{v_2}{r} - \lambda_2^2\frac{v_1}{r} + \frac{\lambda_2\lambda_5}{r} &= 0 \\
\lambda_4^2 + \left(\lambda_1\frac{v_2}{r} - \lambda_2\frac{v_1}{r} + \frac{\lambda_5}{r}\right)^2 &= \frac{\mu}{r^3}\lambda_v^2 - 3\lambda_1^2\frac{\mu}{r^3} \\
(\lambda^2 - 5\lambda_1^2)v_1 + 2v_1(\lambda_1v_1 + \lambda_2v_2) - 4\lambda_1\lambda_4r &= 0.
\end{aligned} \tag{13}$$

### SOLUTIONS FOR LOW-THRUST ARCS

If the final polar angle is not specified and the functional of the problem does not explicitly depend on final polar angle, from the transversality condition we obtain

$$\lambda_5(t_1) = -\frac{\partial J}{\partial \theta(t_1)},$$

hence, it follows that  $\lambda_5(t_1) = C_2 = 0$ . The analytical solutions for this case have been obtained utilizing Eqs. (12)-(13) in terms of the thrust angle and were previously reported in [3] and [9]. In a form that is convenient for application to the planetary capture problem, the analytic solution is given by:

$$\begin{aligned}
r^2 &= \frac{\mu^2}{a^4}s^{\frac{3}{2}} \\
v_1 &= aF_1(s) \\
v_2 &= aF_2(s) \\
\theta &= \frac{1}{4}\left(\frac{3}{\tan \varphi_0} + \varphi_0\right) - \frac{1}{4}\left(\frac{3}{\tan \varphi} + \varphi\right) + \theta_0 \\
\frac{1}{m} &= \frac{1}{m_0} + \frac{P_{max}\lambda_v^2}{2b^2}t \\
I_{sp} &= \frac{2b}{g\lambda_v m} \\
\frac{m_0}{m_f} &= \frac{I_{sp,f}}{I_{sp,0}} \\
t &= \frac{1}{t_c} \left[ \frac{3zk(1-5s)}{3-5s} - \frac{C_1}{\lambda_v} \right] \\
\lambda_1 &= \sqrt{s}\lambda_v \\
\lambda_2 &= k\lambda_v \\
\lambda_4 &= -\frac{k}{r}\sqrt{\frac{\mu}{r}(1-3s)}\lambda_v \\
\lambda_5 &= 0 \\
\lambda_7 &= \frac{b}{m^2}
\end{aligned} \tag{14}$$

where

$$\begin{aligned}
s &= \sin^2 \varphi, & k &= \cos \varphi \\
F_1(s) &= \frac{6s^{\frac{1}{2}}k}{3-5s} \sqrt{\frac{1-3s}{s^{\frac{3}{4}}}} \\
F_2(s) &= \frac{3-s}{3-5s} \sqrt{\frac{1-3s}{s^{\frac{3}{4}}}} \\
z &= \sqrt{\frac{\mu}{r}(1-3s)}.
\end{aligned}$$

The integration constants are computed as follows:

$$\begin{aligned}
a &= \left(\frac{\mu\alpha}{3}\right)^{\frac{1}{4}} \\
\alpha &= \frac{P_{max}}{2} \frac{\lambda_v}{b} - \frac{C}{\lambda_v} \\
\frac{C_1}{\lambda_v} &= \frac{3k_0z_0(1-5s_0)}{3-5z_0} \\
t_c &= \frac{5}{2} \frac{P_{max}\lambda_v}{b} + 3\alpha
\end{aligned} \tag{15}$$

where  $s_0 = \sin^2 \varphi_0$ ,  $k_0 = \cos \varphi_0$ , and  $z_0 = \sqrt{\mu(1-3s_0)/r}$ . The dependency of the flight-path angle  $\psi$  on the thrust angle  $\varphi$  can be found from the analytic solution above to be

$$\tan \psi = \frac{3 \sin 2\varphi}{3 - \sin^2 \varphi}, \tag{16}$$

and it can be shown that, in the case of small thrust angles, we have the approximate expression

$$\tan \psi \approx 2\varphi.$$

Note that the behavior of the flight-path angle in the case of small thrust angle is similar to the corresponding expression for Lawden's spirals which represent IT arcs with constant specific impulse [1]. The analytical solutions presented above will be applied to analyze the capture maneuver in the next section.

### EXAMPLE OF CAPTURE MANEUVER USING LOW-THRUST SOLUTIONS

In this section, we analyze the minimum-fuel capture maneuver for a spacecraft approaching the Earth utilizing the low-thrust analytic solutions obtained in the previous section. It is assumed that, the spacecraft being initially in the heliocentric field, operates its engine to initiate a capture maneuver into the geocentric field. In order to determine the initial conditions, we assume that the spacecraft enters the Earth's gravitational field when magnitude of its radius vector becomes equal or less than radius of sphere of influence ( $r_0 = 9.2482 \times 10^5$  km). As final conditions, the low-thrust maneuver ends with transferring the spacecraft from the low-thrust arc to the given elliptical parking orbit. The time of the transfer is not fixed. We assume that the perigee and apogee (or semi-major axis and eccentricity) of the elliptical parking orbit and final mass of the spacecraft are given. This means, in particular, that the initial true anomaly of the spacecraft on the parking orbit and the orientation of the parking orbit are to be determined. The low-thrust trajectory is to be connected with the elliptical parking orbit in such a manner that all continuity conditions at the junction

must be satisfied. It will be shown below that one low-thrust trajectory can be used to implement the maneuver. The first junction is considered as a starting point of the low-thrust motion and the second junction serves to connect the low-thrust trajectory with the parking orbit. The initial and final values of variables will be denoted by subscripts “1” and “2,” respectively. Forming the continuity conditions at the first and second junctions using Eqn. (14) yields

$$\begin{aligned} r_1 &= \frac{\mu}{a^2} s_1^{\frac{3}{2}} \\ v_{11} &= aF_1(s_1) \\ v_{21} &= aF_2(s_1) \end{aligned} \quad (17)$$

and

$$\begin{aligned} \frac{\mu}{a^2} s_2^{\frac{3}{2}} &= \frac{p}{1 + e \cos f_2} = r_2 \\ aF_1(s_2) &= \sqrt{\frac{\mu}{p}} e \sin f_2 = v_{21} \\ aF_2(s_2) &= \sqrt{\frac{\mu}{p}} (1 + e \cos f_2) = v_{22} \end{aligned} \quad (18)$$

where

$$s_1 = \sin^2 \varphi_1, \quad s_2 = \sin^2 \varphi_2.$$

The functions  $F_1$  and  $F_2$  are given in the previous section. Below we show that the unknowns  $r_1, v_{11}, v_{21}, s_2, \alpha$ , and  $f_2$  are defined as functions of the initial thrust angle,  $\varphi_1$ , semi-latus rectum,  $p$ , and eccentricity,  $e$  (or in the same manner, perigee and apogee) of the parking orbit. Indeed, from Eqs. (17)–(18), the unknowns  $\alpha$  and  $s_2$  may be obtained as functions of  $f_2$  in the form:

$$s_2 = 3 \frac{6 + q^2 - 2\sqrt{6 - 9q^2}}{36 + q^2} \quad \text{and} \quad \alpha = \frac{3}{\mu} \frac{(v_{21}^2 + v_{22}^2)^2}{F_1^2(s_2) + F_2^2(s_2)} \quad (19)$$

with

$$q = \frac{e \sin f_2}{1 + e \cos f_2}.$$

Substituting these expressions into the first expression in Eq. (18) yields a nonlinear equation in terms of the final true anomaly,  $f_2$ :

$$\frac{p}{1 + e \cos f_2} - \sqrt{\frac{3\mu}{\alpha(f_2)}} s_2(f_2)^{\frac{3}{2}} = 0,$$

from which the value  $f_2 = f_2(p, e)$  may be found. This expression indicates that the initial location of the spacecraft on the final orbit will depend only on parameters of this orbit. Then, the unknowns  $r_1, v_{11}$ , and  $v_{21}$  are found directly from Eqs. (17)–(18) as functions of  $\varphi_1$ . Substituting  $f_2(p, e)$  into the relationships in Eq. (19) and using  $s_2 = \sin^2 \varphi_2$  yields

$$\varphi_2(p, e) = \arcsin \sqrt{3 \frac{6 + q^2(p, e) - 2\sqrt{6 - 9q^2(p, e)}}{36 + q^2(p, e)}} \quad (20)$$

and

$$\alpha(p, e) = \frac{3}{p} \frac{1 + e^2 + 2e \cos f_2(p, e)}{F_1^2(\varphi_2(p, e)) + F_2^2(\varphi_2(p, e))}. \quad (21)$$

For the case when the initial range,  $r_1 = r_0$ , is given, the initial thrust angle  $\varphi_1$  can be found from Eqn. (17) to be

$$\varphi_1(p, e) = \arcsin \left[ \frac{a^4 r_0^2}{\mu^2} \right]^{\frac{1}{3}} \quad (22)$$

where

$$a = a(p, e) = \left[ \frac{\mu \alpha(p, e)}{3} \right]^{\frac{1}{4}}.$$

Substituting the values of  $\varphi_1$  and  $a$  into Eq. (17) yields the components of the initial velocity of the low-thrust trajectory that will satisfy the conditions at the first junction, namely

$$v_{11} = v_{11}(p, e, r_0) = a(p, e)F_1(p, e, r_0), \quad (23)$$

and

$$v_{21} = v_{21}(p, e, r_0) = a(p, e)F_2(p, e, r_0). \quad (24)$$

Then, the final polar angle can be computed using Eq. (14) in the form:

$$\theta_2 = \theta_2(p, e, r_0) = \frac{1}{4} \left( \frac{3}{\tan \varphi_1(p, e, r_0)} + \varphi_1(p, e, r_0) \right) - \frac{1}{4} \left( \frac{3}{\tan \varphi_2(p, e)} + \varphi_2(p, e) \right) + \theta_1. \quad (25)$$

The number of revolutions of the spiral trajectory around the center of attraction may be computed via:

$$N_{rev} = \frac{\theta_2(p, e, r_0)}{2\pi}.$$

Consequently, the orientation of the parking orbit is defined as

$$\omega = \theta_2(p, e, r_0) - f_2(p, e). \quad (26)$$

It should be noted that the constant  $\alpha$  is specified by the semi-latus rectum,  $p$ , and eccentricity,  $e$ , of the final orbit. This constant is common between the systems Eqs. (17)–(18) and permits us to compute the terminal kinematic characteristics of the transfer, that is, the initial and final position and velocity vectors including the orientation of the parking orbit and the number of revolutions of the spiral trajectory.

If the final mass,  $m_2$ , the maximum level of power,  $P_{max}$ , the flight time,  $t_2$ , are specified, then all constants, initial mass,  $m_1$ , initial and final values of specific impulse,  $I_{sp1}$ ,  $I_{sp2}$ , respectively, can be found as functions of  $p, e, r_0, m_2, P_{max}$ , and  $t_2$  as follows:

$$\begin{aligned} \frac{\lambda_v}{b} &= \frac{2}{5P_{max}} \left( \frac{d}{t_2} - 3\alpha \right) \\ \frac{C}{\lambda_v} &= \frac{P_{max}}{2} \frac{\lambda_v}{b} - \alpha \\ \frac{C_1}{\lambda_v} &= \frac{3k_1 z_1 (1 - 5s_1)}{3 - 5z_1} \\ m_1 &= \left[ \frac{1}{m_2} - \frac{P_{max}}{2b} t_2 \lambda_v^2 \right]^{-1} \\ I_{sp1} &= \frac{2}{g_0 m_1} \frac{b}{\lambda_v} \end{aligned}$$

$$\begin{aligned}
I_{sp2} &= \frac{2}{g_0 m_2} \frac{b}{\lambda_v} \\
\beta_1 &= \frac{2P_{max}}{I_{sp1}^2 g^2} \\
\beta_2 &= \frac{2P_{max}}{I_{sp2}^2 g^2} \\
a &= \frac{I_{sp1} g \beta_1}{m_1} = \text{constant} \\
J &= \frac{1}{2} a^2 t_2
\end{aligned}$$

where

$$\begin{aligned}
d &= \frac{3z_2 k_2 (1 - 5s_2)}{3 - 5s_2} - \frac{C_1}{\lambda_v} \\
z_1 &= \sqrt{\frac{\mu}{r_1} (1 - 3s_1)} \\
z_2 &= \sqrt{\frac{\mu}{r_2} (1 - 3s_2)} \\
k_1 &= \cos \varphi_1, \quad k_2 = \cos \varphi_2 \\
t_c &= \frac{5}{2} P_{max} \frac{\lambda_v}{b} + 3\alpha
\end{aligned}$$

## NUMERICAL RESULTS

As mentioned in the previous section, by specifying  $p$ ,  $e$ , and  $r_0$ , and consequently, finding  $\alpha$  (or  $a$ ), one can obtain the initial and final position vector  $(r, \theta)$  and velocity vector  $(v_1, v_2)$ , initial and final thrust angles  $(\varphi_1, \varphi_2)$ , longitude of perigee,  $\omega$ , and the number of revolutions,  $N_{rev}$ , of the capture spiral. The solutions presented in this paper show that these values are independent of the dynamical characteristics of the maneuver, namely  $P_{max}, I_{sp}, m, \beta, a$ , and  $J$ . Following the solution process described in the previous section and specifying  $r_{min} = 6870$  (corresponding to  $h_0 = 500$ ), and  $r_{max} = 6880$  (corresponding to  $p = 6874$  and  $e = 0.00072$  for the parking orbit), we find the final true anomaly on the LT trajectory and thrust angle, that is,  $f_2 = -1.5708$ ,  $\varphi_2 = -0.00036$ , and consequently,  $\alpha = 1.2165 \times 10^{-12}$ . Then, by specifying the initial range,  $r_1 = r_0$ , the initial thrust angle is found to be  $\varphi_1 = -0.0095$ . After  $\alpha, \varphi_1, \varphi_2$  are found, it can be shown that

$$\begin{aligned}
v_{11} &= -0.0125, \quad v_{12} = -0.0055 \\
v_{21} &= 0.6565, \quad v_{22} = 7.6143 \\
\omega &= 4.2502, \quad N_{rev} = 315.75
\end{aligned}$$

The corresponding integration constant is  $C_1/\lambda_v = 0.65619$ . Then, by specifying  $t_2, m_2$ , and  $P_{max}$ , one can compute the other variables of the maneuver. Note that  $P_{max}$  includes the efficiency of the propulsion system, denoted by  $e_{eff}$ . Several sets of computations have been implemented in order to analyze the behavior of various parameters of the maneuver. In the first set of computations, the following intervals are considered:  $30 \leq t_2 \leq 180$  days,  $3 \leq P_{max} \leq 12$  kw; and  $200 \leq m_2 \leq 600$  kg. In order to change the parameters of the parking orbit, the apogee distance is varied in the interval  $6880 \leq r_{max} \leq 7370$  km. In particular, for the case when  $t_2 = 120, m_2 = 600, P_{max} = 3, e_{eff} = 0.6$  and  $r_{min} = 6870$ ,

Table 1: Numerical results:  $t_2 = 120$  days,  $m_2 = 600$  kg,  $P_{max} = 3$  kw,  $e_{eff} = 0.6$ ,  $r_{min} = 6870$  km

$r_{max}$	$\sin^2 \varphi_1$	$\sin^2 \varphi_2$	$m_1$	$I_{sp1}$	$I_{sp2}$	$\beta_1$	$\beta_2$	$J/g^2$
6880	9.1e-05	1.323e-07	685.342	1994.66	2278.37	9.4e-06	7.206e-06	0.003881
6890	0.00036	5.281e-07	685.284	1995.43	2279.06	9.39e-06	7.201e-06	0.00388
6910	0.00144	2.106e-06	685.175	1996.85	2280.32	9.38e-06	7.194e-06	0.00387
6950	0.00573	8.377e-06	684.821	2001.53	2284.49	9.33e-06	7.167e-06	0.00386
6990	0.01278	1.874e-05	683.971	2012.89	2294.60	9.23e-06	7.104e-06	0.00382
7050	0.02835	4.180e-05	681.028	2053.55	2330.87	8.87e-06	6.885e-06	0.00370
7130	0.05805	8.623e-05	672.660	2182.02	2446.26	7.85e-06	6.251e-06	0.00336
7210	0.09743	0.00014	658.495	2457.91	2697.54	6.19e-06	5.140e-06	0.00276
7330	0.17349	0.00026	629.467	3542.00	3715.96	2.98e-06	2.709e-06	0.00145
7370	0.20311	0.00030	619.540	4384.33	4527.20	1.94e-06	1.825e-06	0.00098

the results, presented in Table 1, have been obtained by varying the apogee distance,  $r_{max}$ . The value of eccentricity that corresponds to the values of  $r_{max}$  shown in Table 1 varies from  $e = 0.0007272$  to  $e = 0.03511$ .

It can be seen from the data in Table 1 that as the parking orbit becomes more elliptical, the maneuver becomes more effective and the optimal specific impulse increases. It can be shown also that in this case the number of revolutions decreases from  $N_{rev} = 315.75$  to  $N_{rev} = 6.54$  and the initial thrust angle,  $\varphi_1$  approaches the trajectory tangential direction. Analysis show that initial velocity and the number of revolutions are sensitive to changes in initial thrust angle as illustrated in Fig. 1 and 2. Using the results of the previous section, we note that this dependency is not sensitive to changes in the parameters of parking orbit.

It can be observed from Table 1 and Fig. 3 that while the spacecraft is spiraling, the thrust angle and total velocity increase. It is important to note that each set of the perigee and apogee of the parking orbit and the initial range specify the shape of spiral trajectory and number of revolutions that are not dependent on other parameters of the maneuver. This can be seen from the Fig. 4 and Fig. 5 that have been generated for  $e = 0.000727$  and  $e = 0.0303$ . It can be shown that an increase of the eccentricity by more than forty-five times results in reducing the  $N_{rev}$  from about 315 to 4.5. The computations have been implemented for values of maximum power from 3 kw to 12 kw and for final mass from 200 kg to 600 kg.

The solutions presented in the previous section permit us to generate time histories of all variables at different values of maximum power and final mass. The time histories of mass and specific impulse are shown in Fig. 6 and Fig. 7 for  $P_{max} = 3$  kw and  $m_1 = 300$  kg. The Fig. 6 shows almost linear relationship between time of flight and the current mass. The same relationship can be observed in Fig. 7 between the specific impulse and the flight time allowing us to conclude that the optimal specific impulse is almost constant as the flight time is increases. The same qualitative notes can be made from such dependencies for other values of power and final mass.

Figures 8, 9, and 10 have been generated to show the relationships of the initial values of specific impulse, mass and thrust acceleration with power as independent variable while fixing times of flight and parameters of parking orbit. The plots show that higher values of power will result in higher values of the specific impulse, lower values of the initial mass, and lower and constant values of the thrust acceleration while the flight duration increases.

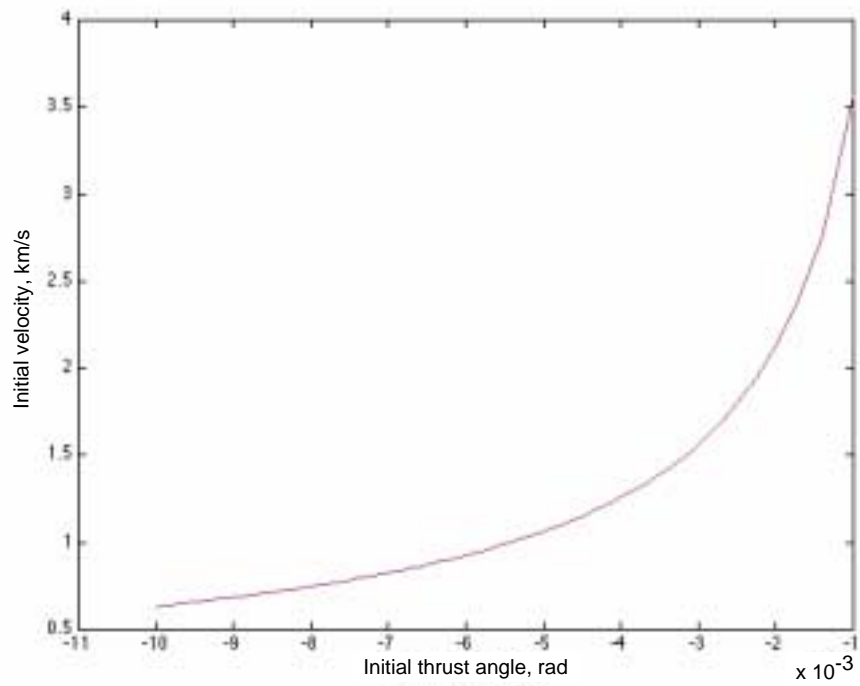


Figure 1: Initial velocity versus initial thrust angle for  $e = 0.0007272$  and  $p = 6874$  km.

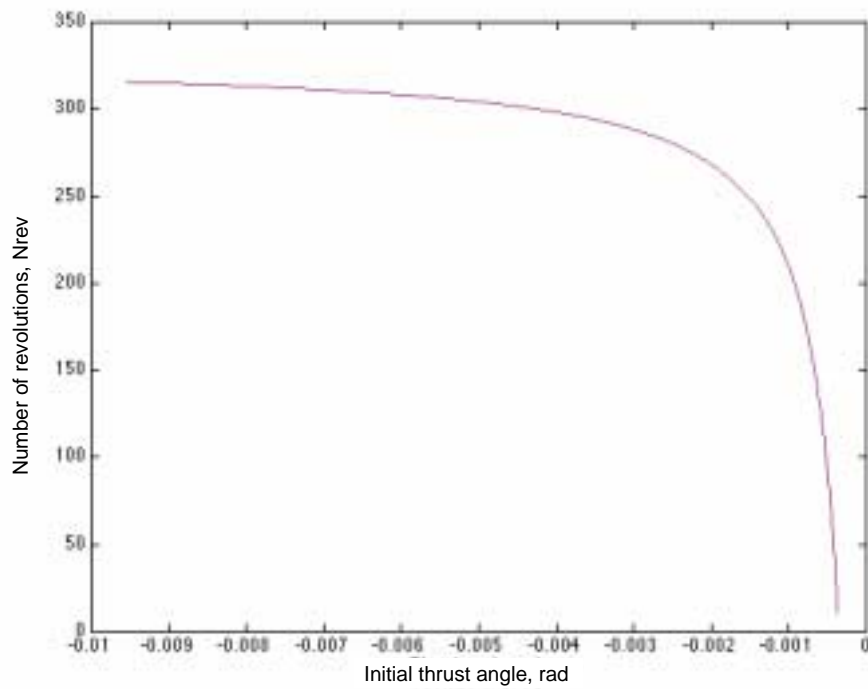


Figure 2: Number of spiral revolution versus initial thrust angle for  $e = 0.0007272$  and  $p = 6874$  km.

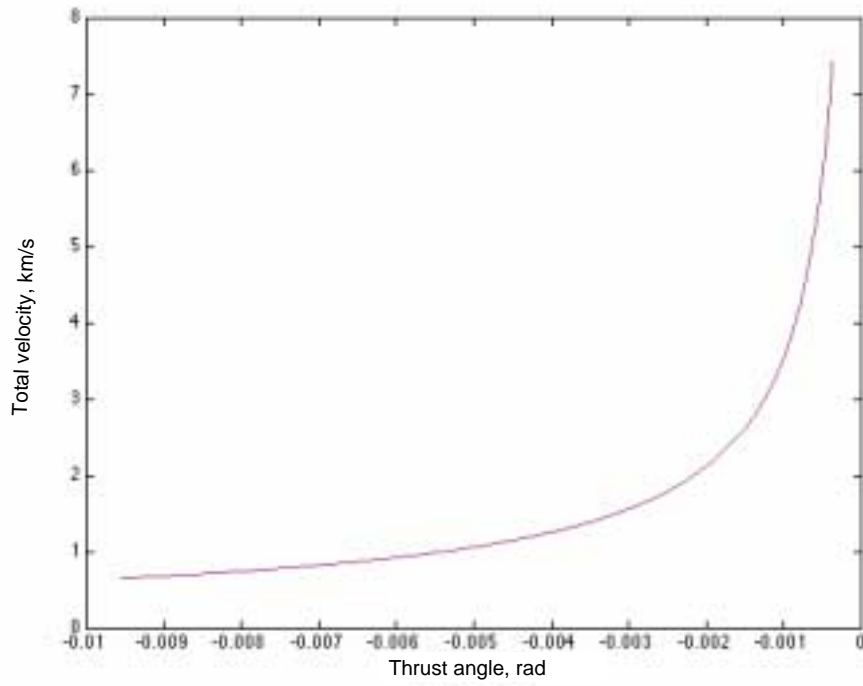


Figure 3: Thrust angle  $\varphi$  vs  $v_{total}$  for  $e = 0.0007272$  and  $p = 6874$  km.

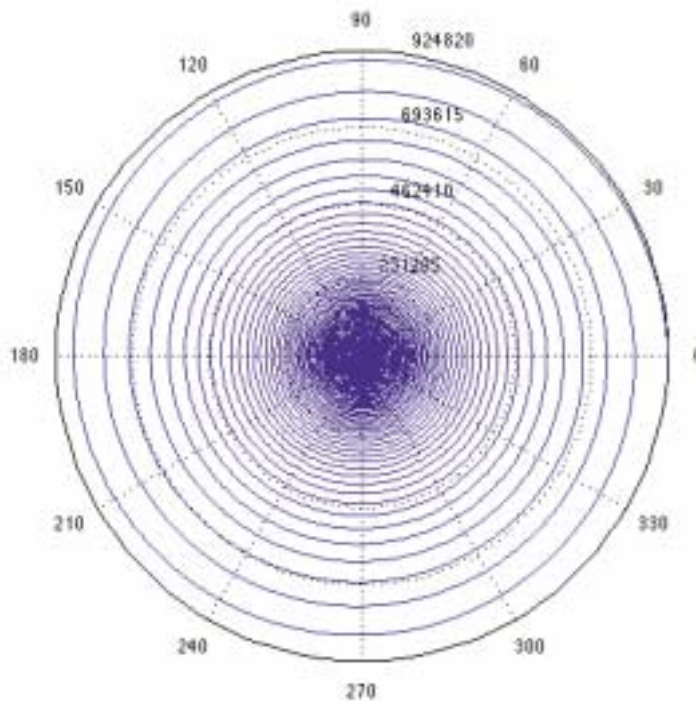


Figure 4: Capture spiral trajectory for  $r_1 = r_0$ ,  $e = 0.0007272$ , and  $p = 6874$  km.

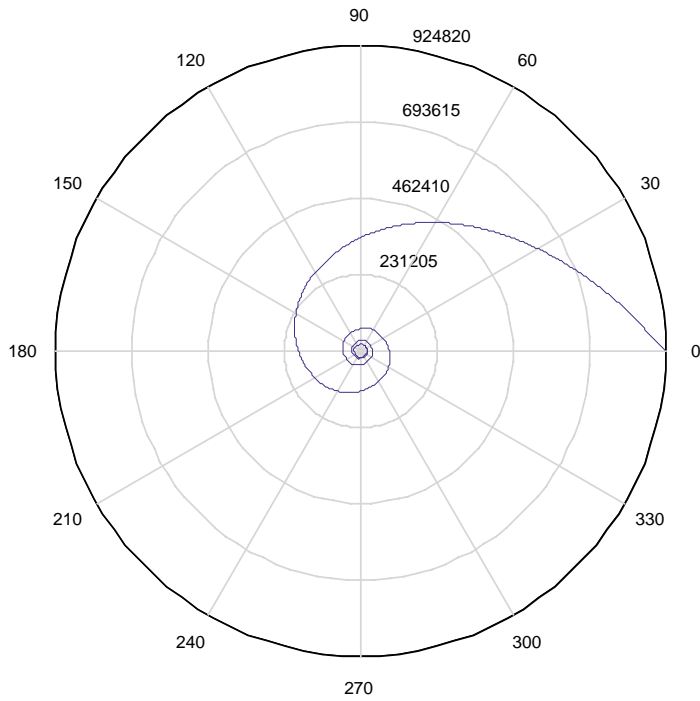


Figure 5: Capture spiral trajectory for  $r_1 = r_0$ ,  $e = 0.0303$ , and  $p = 20031.59$  km.

$m_1 = 300$  kg;  $P = 3$  KW;  $a = 20000.005$ ;  $b = 20000$  km

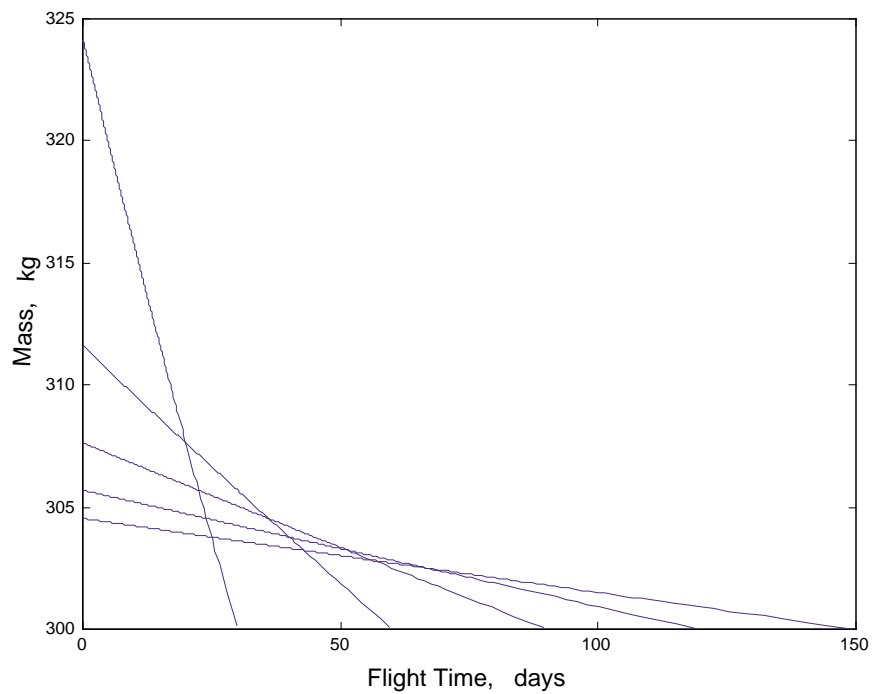


Figure 6: Time history of the spacecraft mass.

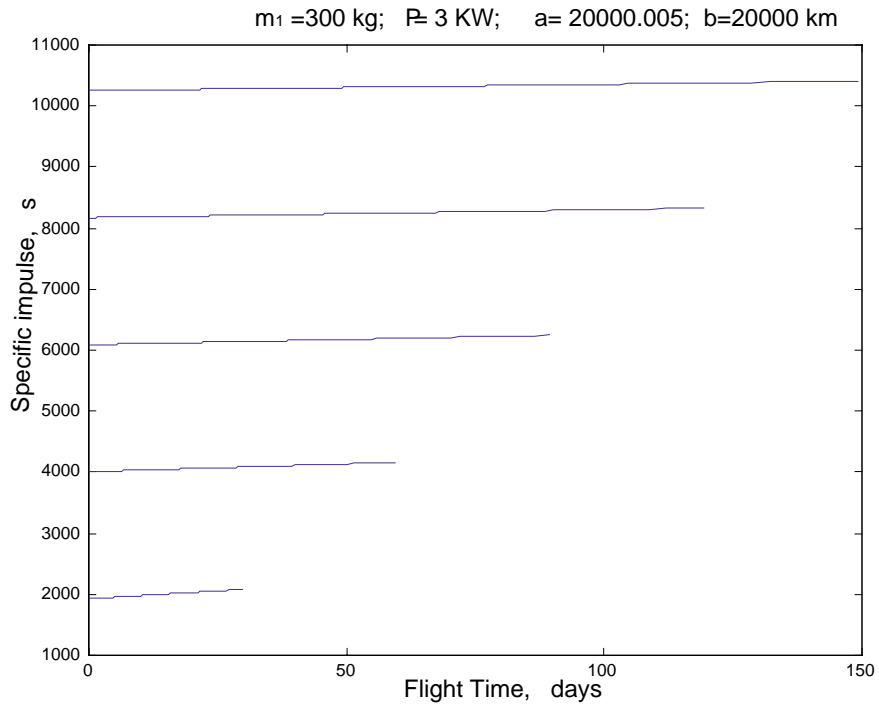


Figure 7: Time history of the specific impulse.

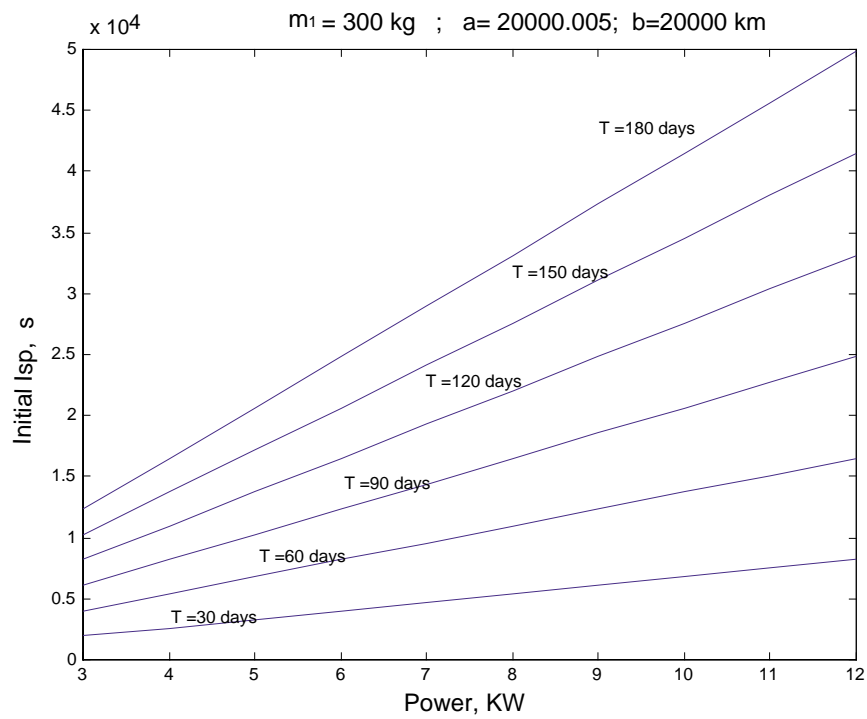


Figure 8: Initial specific impulse versus maximum power.

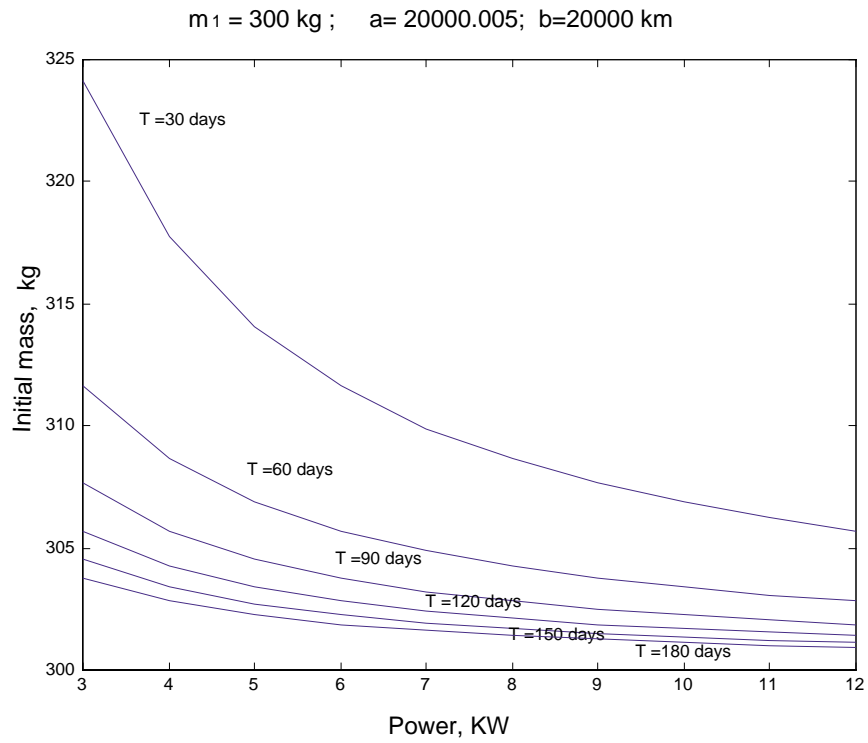


Figure 9: Initial mass versus maximum power.

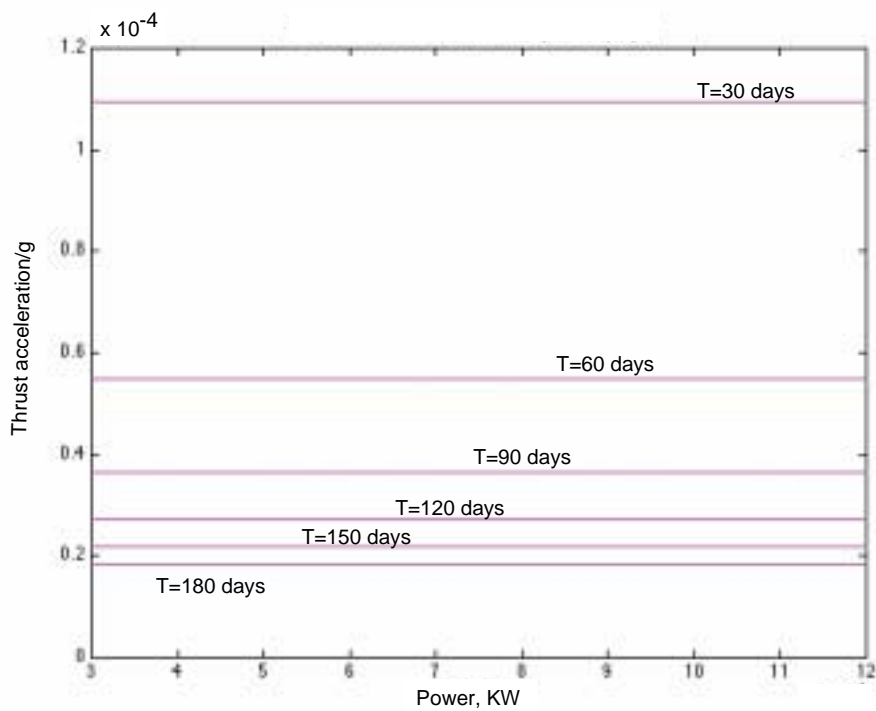


Figure 10: Thrust acceleration versus maximum power.

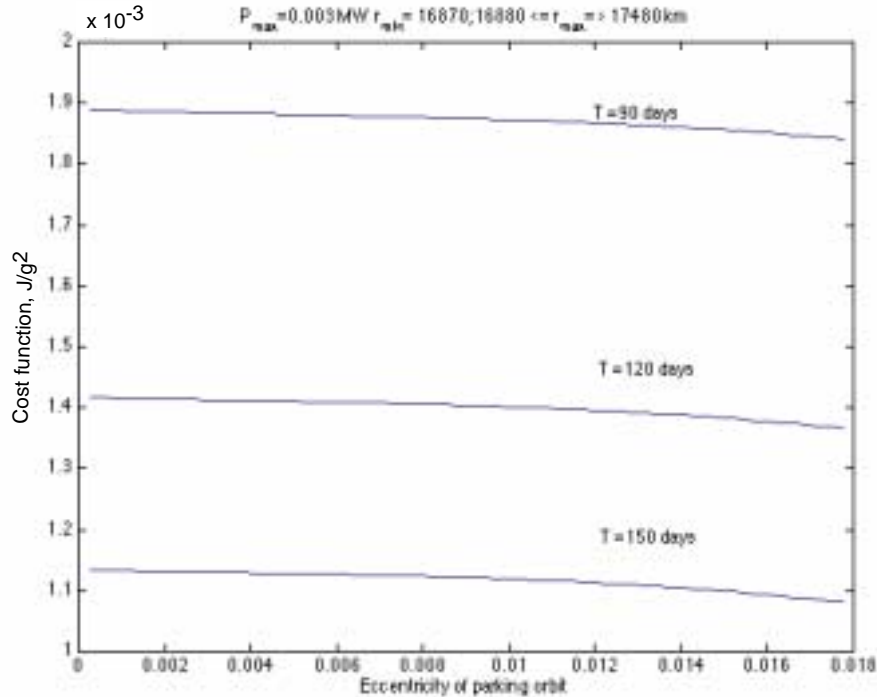


Figure 11: Cost function versus eccentricity of parking orbit at various flight times.

The final set of computations show the behavior of the parameters of the low-thrust maneuver while the eccentricity of parking orbit varies. Figures 11 and 12 show the behavior and sensitivity of the cost function to changes in eccentricity and in the shape of the parking orbit by increasing apogee distance. The cost can be minimized by choosing the largest eccentricity and highest apogee. Near-circular parking orbits result in higher values of the cost and larger number of spiral revolutions.

Figures 13–15 show that by specifying a higher parking orbit or by increasing the eccentricity (or apogee), the initial mass flow-rate and cost function can be decreased, while allowing initial specific impulse to increase slowly and almost linearly. But if the perigee and apogee are lower, the initial specific impulse becomes more sensitive to small changes in the eccentricity. It is important to note that the solutions for LT arcs being used in this problem can not be used to the capture to exactly circular parking orbits with zero eccentricity.

## CONCLUSIONS

The variational problem of determining optimal trajectories of spacecraft equipped with power-limited propulsion systems has been considered. Analytical solutions to the problem were presented in a convenient form for further applications, in particular, in order to use them to determine low-thrust capture maneuvers. These solutions describe motion with low-thrust variable specific impulse and maximum level of power along spiral trajectories around a center of attraction. Illustrative examples of optimal low-thrust capture maneuvers were used to demonstrate the solutions. The computations with various sets of parameters permit us to conclude that planetary capture maneuvers can be analyzed using the analytical solutions for low-thrust motion presented in this paper.

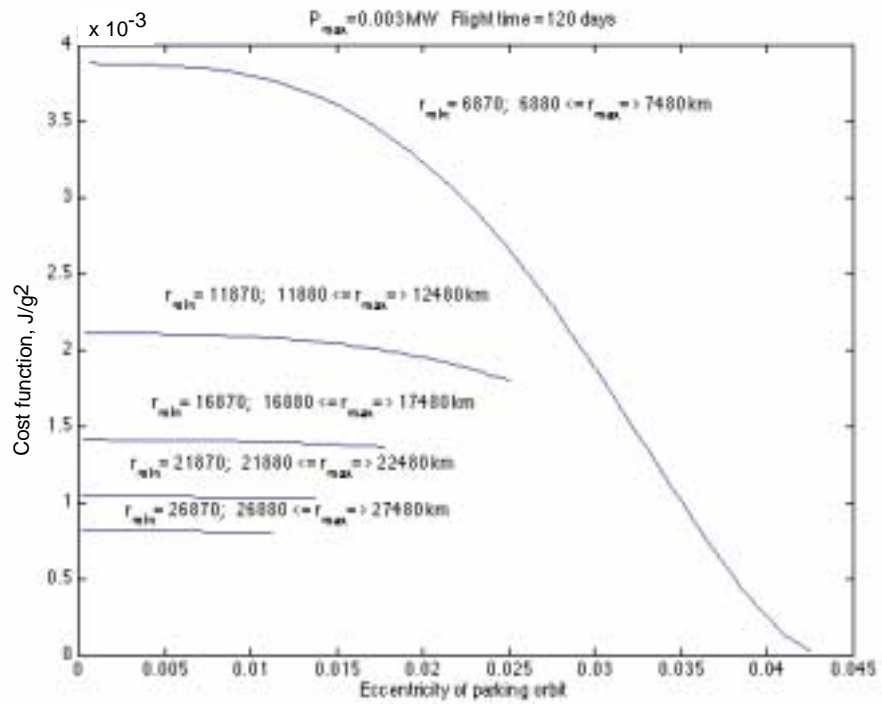


Figure 12: Cost function versus eccentricity of parking orbit at various apogees.

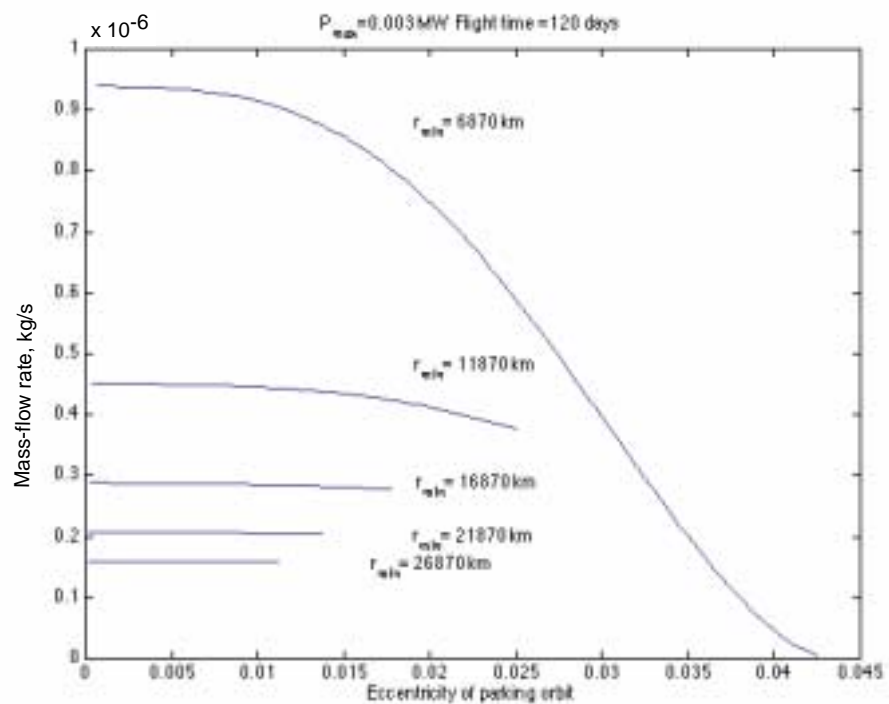


Figure 13: Mass-flow rate versus eccentricity of parking orbit at various apogees.

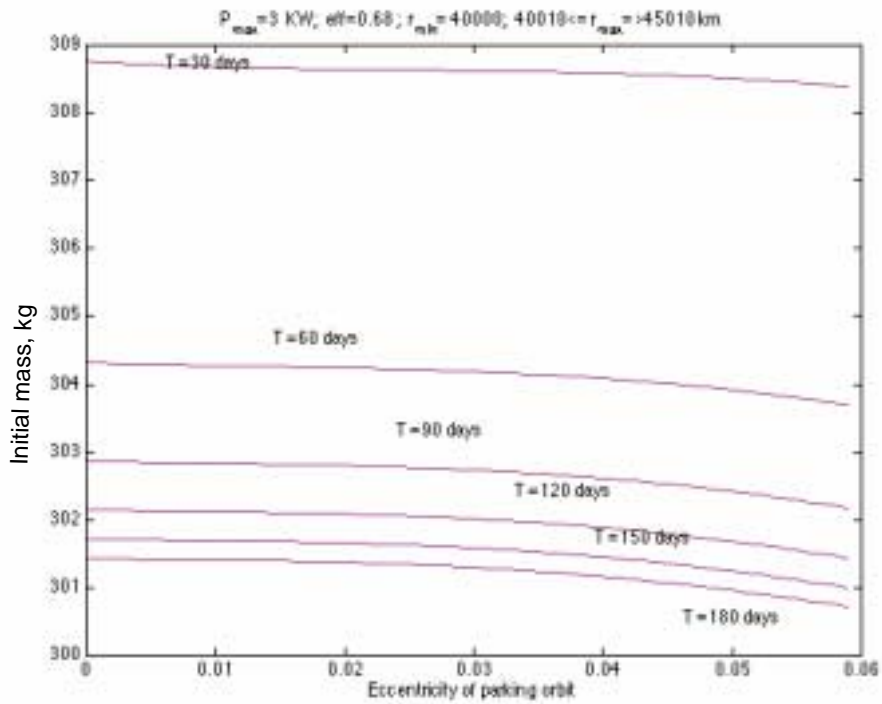


Figure 14: Initial mass versus eccentricity of parking orbit.

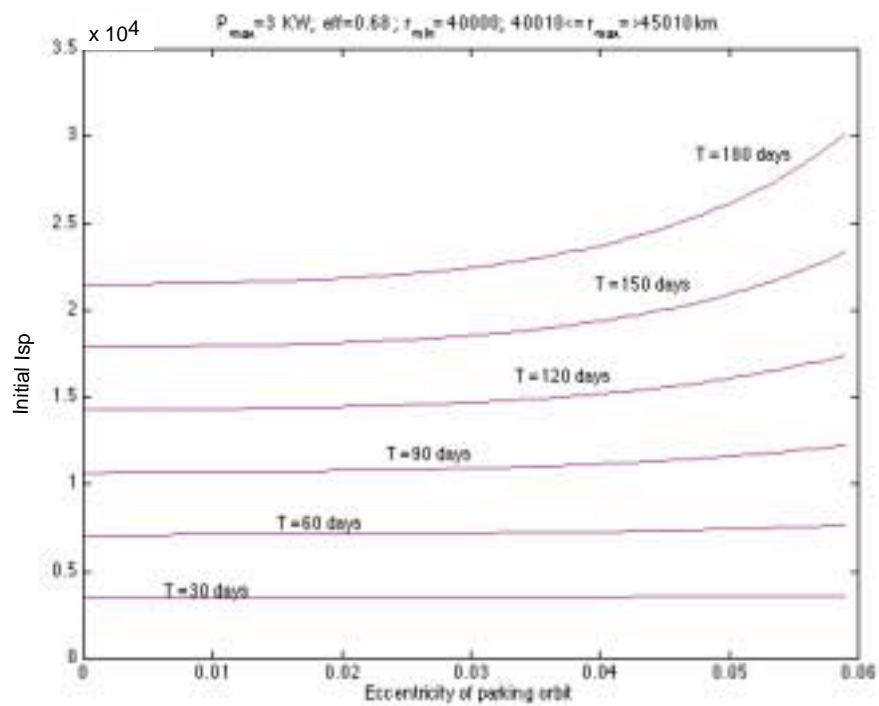


Figure 15: Initial specific impulse vs eccentricity of parking orbit

## ACKNOWLEDGEMENTS

The work described in this paper was carried out at The University of Texas at Austin under contract to the NASA Johnson Space Center. The work of the authors was supported by NASA grant NAG9-1323. Special thanks to Dr. Timothy Crain for his contributions to and oversight of this project.

## REFERENCES

- [1] Lawden, D. F., *Optimal Trajectories for Space Navigation*, Butterworths, London, 1963, pp. 55-99.
- [2] Melbourne, W. G., and Sauer, C. G., Jr., "Optimum Thrust Programs for Power-Limited Propulsion Systems," *Acta Astronautica*, Vol. 8, No. 4, 1962, pp. 205-227.
- [3] Bishop R.H., Azimov, D.M. "Analytical trajectories of an extremal motion with Low-Thrust Exhaust-Modulated Propulsion" *AIAA Journal of Guidance, Control and Dynamics* (in print)
- [4] Kluever, C. A., "Optimal Low-Thrust Interplanetary Trajectories by Direct Method Techniques," *The Journal of the Astronautical Sciences*, Vol. 45, No. 3, 1997, pp. 247-262.
- [5] Tang, S. and Conway, B. A., "Optimization of Low-Thrust Interplanetary Trajectories Using Collocation and Nonlinear Programming," *Journal of Guidance, Control and Dynamics*, Vol. 18., No. 3, 1995, pp. 599-604.
- [6] Chang-Diaz, F. R., Hsu, M. M., Braden, E., Johnson, I., and Yang T. F., "Rapid Mars Transits With Exhaust Modulated Plasma Propulsion," *NASA Technical Paper*, No. TN-3539, 1995.
- [7] Braden, E. M., Cockrell, B. F., Bordano, A. J., "Power-Limited Human Mission to Mars," Lyndon B. Johnson Space Center, Aerospace and Flight Mechanics Division, No. JSC-28436, Sept. 1998, pp. 1-35.
- [8] Vadali, S. R., Nah, R., Braden, E. and Johnson, I. L., Jr., "Fuel-Optimal Planar Interplanetary Trajectories Using Low-Thrust Exhaust -Modulated Propulsion," *AIAA/AAS Paper 99-132*, 7-10 Feb. 1999.
- [9] Azimov, D. M., "A New Classes for Intermediate-Thrust Arcs of Flight Trajectories in a Newtonian Field," *AIAA Journal of Guidance, Control and Dynamics*, Vol. 23, No. 1, 2000, pp. 142-145.